AGU PUBLICATIONS

Water Resources Research

RESEARCH ARTICLE
10.1002/2015WR017972

Spatiotemporal processes that contribute to hydrologic exchange between hillslopes, valley bottoms, and streams

Anna Bergstrom[1], Kelsey Jencso[1], and Brian McGlynn[2]

[1]Department of Forest Management, College of Forestry, University of Montana, Missoula, Montana, USA, [2]Division of Earth and Ocean Sciences, Nicholas School of the Environment, Duke University, Durham, North Carolina, USA

Key Points:
- Lateral contributing area, underlying lithology, and vegetation density organize stream hydrologic gains
- High step frequencies along stream reaches increased gross hydrologic losses
- Topography, geology, and stream morphology organize the stream water balance

Correspondence to:
A. Bergstrom,
abergst@gmail.com

Citation:
Bergstrom, A., K. Jencso, and B. McGlynn (2016), Spatiotemporal processes that contribute to hydrologic exchange between hillslopes, valley bottoms, and streams, *Water Resour. Res.*, *52*, doi:10.1002/2015WR017972.

Received 7 AUG 2015
Accepted 20 MAY 2016
Accepted article online 26 MAY 2015

Abstract Quantifying how watershed structure influences the exchanges of water among component parts of a watershed, particularly the connection between uplands, valley bottoms, and in-stream hydrologic exchange, remains a challenge. However, this understanding is critical for ascertaining the source areas and temporal contributions of water and associated biogeochemical constituents in streams. We used dilution gauging, mass recovery, and recording discharge stations to characterize streamflow dynamics across 52 reaches, from peak snowmelt to base flow, in the Tenderfoot Creek Experimental forest, Montana, USA. We found that watershed-contributing area was only a significant predictor of net changes in streamflow at high moisture states and larger spatial scales. However, at the scale of individual stream reaches, the lateral contributing area in conjunction with underlying lithology and vegetation densities were significant predictors of gross hydrologic gains to the stream. Reach lateral contributing areas underlain by more permeable sandstone yielded less water across flow states relative to those with granite gneiss. Additionally, increases in the frequency of steps across each stream reach contributed to greater hydrologic gross losses. Together, gross gains and losses of water along individual reaches resulted in net changes of discharge that cumulatively scale to the observed outlet discharge dynamics. Our results provide a framework for understanding how hillslope topography, geology, vegetation, and valley bottom structure contribute to the exchange of water and cumulative increases of stream flow across watersheds of increasing size.

1. Introduction

Quantifying how watershed structure and organization influences the redistribution of precipitation between hillslopes valley bottoms, and streams has been a continuous research theme in watershed hydrology [e.g., *Horton*, 1914; *Hewlett and Hibbert*, 1967; *Uchida et al*., 2005]. In order to address this challenge, many studies have identified the factors that organize runoff and streamflow dynamics from individual experimental hillslopes, stream reaches, or at the scale of entire watersheds. However, we have yet to develop a framework to quantify the relative role of these factors for stream discharge across spatial scales and differing wetness states [*Dooge*, 1986; *Blöschl and Sivapalan*, 1995; *Bonell*, 1998; *McDonnell et al*., 2007; *Wagner et al*., 2007]. This context is necessary for improving our estimates of the timing and magnitude of streamflow as well as hydrologic exchange, biogeochemical cycling, and watershed sensitivity to climate change across differing settings.

In order to better quantify the role of landscape structure for runoff generation at smaller scales, many studies have focused on landscape discretization of watersheds into hillslopes, riparian areas (valley bottoms), and stream networks [*Sidle et al*., 2000; *McGlynn and Seibert*, 2003; *McGlynn et al*., 2004; *Jencso et al*., 2009]. At the hillslope scale, the timing and magnitude of water delivery from uplands to streams has been described in terms of hydrologic connectivity: the development of shallow subsurface flow that leads to water table continuity across hillslope, riparian, and stream landscape positions [*McGlynn et al*., 2004; *Jencso et al*., 2009]. Recent work has shown that the duration of hydrologic connectivity between hillslopes and adjacent stream reaches can be related to upslope contributing area [*Jencso et al*., 2009]. As antecedent moisture conditions decrease, hillslope contributing areas can become disconnected from their adjacent valley bottoms and the channel network [*Jencso et al*., 2009; *Smith et al*., 2013; *Nippgen et al*., 2015]. During drier time periods the difference between the total watershed area and the actual watershed area that is actively contributing water to streamflow increases [*D'Odorico and Rigon*, 2003; *Jencso et al*., 2009; *Smith*

© 2016. American Geophysical Union. All Rights Reserved.

et al., 2013; *Nippgen et al*., 2011, 2015]. With the exception of a few large hillslopes, low flows may be largely derived from storage in the valley bottom or riparian areas [*Jencso et al*., 2010] and/or deeper groundwater contributions [*Hornberger et al*., 1998].

Beyond hydrologic connectivity in the shallow subsurface, hydrogeologists have long considered nested geologic flow pathways and how they might reemerge as streamflow [i.e., *Toth*, 1963]. Previous investigations [*Onda et al*., 2001; *Uchida et al*., 2005] and recent studies performed in benchmark experimental hillslopes where bedrock had previously been assumed to be impermeable (e.g., Panola and MaiMai) have indicated significant potential for the exchange of water between the shallow subsurface and underlying bedrock [*Graham et al*., 2010; *Gabrielli et al*., 2012; *Tromp-van Meerveld et al*., 2007]. These studies suggest that the underlying lithology of a watershed may act as either a sink or source for shallow subsurface flow across different time scales [*Generaux et al*., 1993; *Tague and Grant*, 2004; *Jencso and McGlynn*, 2011; *Payn et al*., 2012; *Creutzfeldt et al*., 2014].

In near stream areas where deeper groundwater flow and shallow subsurface flow from the uplands likely converge, valley bottoms, riparian zones, and stream geomorphology may play a disproportionate role (due to their relative extents) in the transfer of water between uplands and stream networks [*McGlynn et al*., 2004; *Jencso et al*., 2010]. Across a given stream reach, water can enter and leave the channel [*Kennedy et al*., 1984; *Triska et al*., 1989; *Harvey and Bencala*, 1993; *Harvey et al*., 1996; *Payn et al*., 2009] resulting in hydrologic exchange. The degree of exchange has been related to streamflow velocity [*Covino et al*., 2011; *Mallard et al*., 2014] and channel and valley bottom storage states [*Harvey et al*., 1996; *Ward et al*., 2012]. Both stream flow velocity and storage state are dynamic in space and time and have been found to be influenced by channel and valley bottom structure [*Harvey and Bencala*, 1993; *Vidon and Smith*, 2007; *Payn et al*., 2009; *Ward et al*., 2014]. Structural features in the valley bottom that affect the channel water balance occur over a range of scales and also can be dependent on the underlying lithology of the reach [*Bencala et al*., 2011].

Hydrologic exchange potential can be quantified by gross gains and losses of water over a reach and has been used to examine valley bottom function, particularly for biogeochemical cycling in the hyporheic zone [*Hayashi and Rosenberry*, 2002]. Gross gains and losses are often studied together as hyporheic exchange. While exchange and the extent of the hyporheic zone have been considered in the context of dynamic valley hydraulic gradients through watershed moisture states [e.g., *Ward et al*., 2012] these analyses are typically constrained to the valley bottom [e.g., *Harvey and Bencala*, 1993; *Triska et al*., 1989; *Payn et al*., 2009; *Ward et al*., 2014]. It remains unclear how inputs of water from adjacent hillslopes may influence spatial patterns and magnitudes of stream gains and losses. Furthermore, field and modeling studies of hydrologic exchange typically only consider one or two reaches and rarely incorporate continuous reaches across a stream network.

Discharge measured at the outlet or at any point along the stream network of a watershed is an integration of exchanges between flow pathways across a wide range of spatial and temporal scales. This study aims to advance our understanding of how these processes are integrated across a watershed. To this end, we ask: How does watershed structure influence the gains and losses (hydrologic exchange) of water between hillslopes, valley bottoms, and streams across space and time? In order to address this question we measured streamflow at high spatial and temporal resolution in 52 reaches across the Tenderfoot Creek Experimental Forest (TCEF) in the 2013 water year. In addition, we performed mass recovery experiments across four flow states to measure the gross channel water balance in 14 reaches of one subwatershed. Using these observations, we developed a framework for evaluating the evolving controls on streamflow timing and magnitude from the reach to watershed scales.

2. Site Description

2.1. General Description and Climate

The Tenderfoot Creek Experimental Forest (TCEF) is located in the Little Belt mountains of central Montana (Figure 1; latitude: 46°55′N, longitude: 110°52′W) which are headwaters of the Smith River, a tributary of the Missouri River. The TCEF is subalpine with an elevation range of 1838–2421 m. There are 11 subwatersheds, which compose the larger Tenderfoot Creek watershed (22.8 km^2; Figure 1). This research focused on the main stem of Tenderfoot Creek and four of the subwatersheds: Bubbling (3.1 km^2), Sun (3.6 km^2), Spring Park (4 km^2), and Stringer (5.5 km^2).

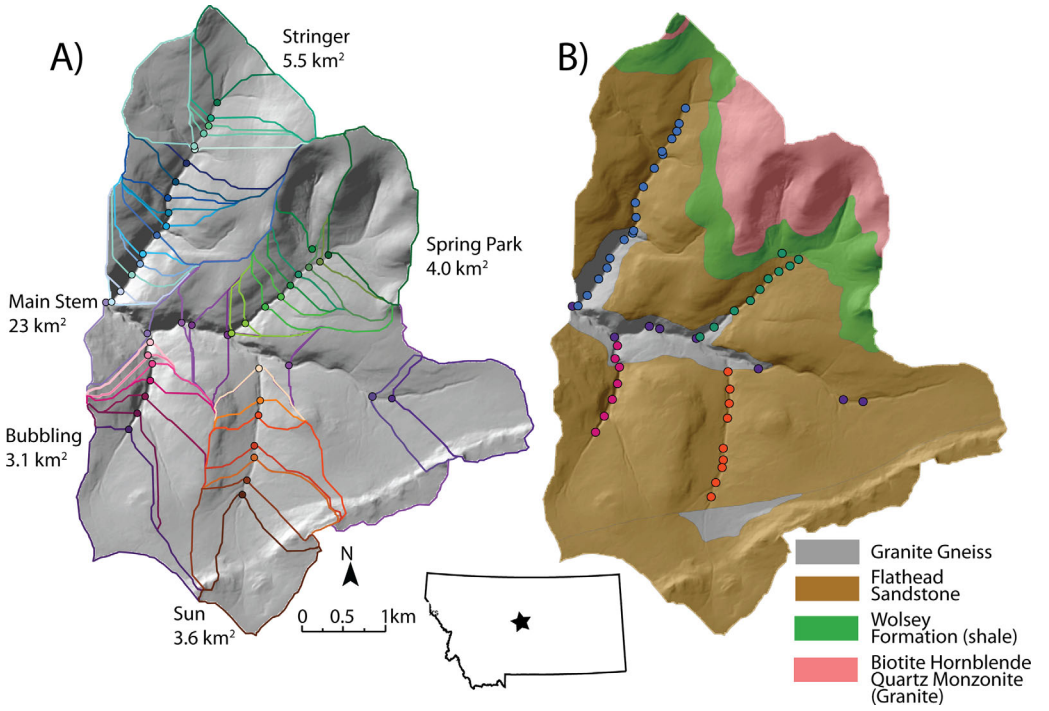

Figure 1. (a) Site map and location of the Tenderfoot Creek Experimental Forest. Points on the map represent locations of the stilling wells and flumes where discharge was measured. Lines represent the contributing area to each discharge measurement point. Each subwatershed is signified by a color. Stringer: blue, Spring Park: green, Sun: orange, Bubbling: pink. Lighter shades of each watershed indicate stilling wells closer to the watershed outlet. This color convention is used in subsequent figures. (b) Geologic map of the TCEF [after *Reynolds*, 1995] with points at stilling wells and flumes.

The climate of the TCEF is continental with a periodic maritime influence. *Nippgen et al*. [2011] calculated an elevation weighted average annual precipitation at the TCEF of 790 mm (1996–2009 water years), 70% of which occurs in the form of snow. Peak precipitation typically occurs in the winter as snow which results in a snowmelt dominated hydrologic response. Peak flows occur during snowmelt in May through early June and recede to base flow by mid to late July. Base flow continues through the fall and winter but is punctuated by small flow increases in September–October until a continuous snowpack develops. The average annual temperature is 1.4°C. In the 2013 water year (when this study was conducted) the TCEF received a total of 940 mm of precipitation (Natural Resources Conservation Service SNOTEL Site #1008, Onion Park).

Vegetation at the TCEF is dominated by Lodgepole pine (*Pinus contorta*) with limited subalpine fir (*Abies lasiocarpa*) and Engelman spruce (*Picea engelmannii*) [*Mincemoyer and Birdsall*, 2006]. Four percent of the watershed area is considered riparian [*Jencso et al*., 2009]. Upland meadows or parks make up 5.3% of the watershed area [*Schmidt and Friede*, 1996]. Two subwatersheds: Sun and Spring Park underwent harvesting treatments in 2000 in the form of stand thinning and patch cutting over a total of 764 ha. The treated area in the Spring Park watershed totaled 127 ha or 32% of the watershed area. In Sun 162 ha were treated, 45% of the watershed area [*Hood et al*., 2012].

2.2. TCEF Soils and Lithology

Soils at the TCEF are relatively homogenous (0.5–1.5 m in depth) [*Jencso et al*., 2009] with localized areas of deeper soils in upslope locations. Hillslope soils are typically loamy skeletal, mixed typic Cryochrepts. Riparian and park soils are clayey, mixed Aquic Cryoboralfs [*Holdorf*, 1981]. The geologic characterization of the TCEF watersheds is based on United States Geological Service (USGS) surveys [*Reynolds*, 1995]. Three main rock types underlie the TCEF: Gneiss, Flathead Sandstone, and Woolsey Shale (Figure 1). We verified and mapped the location of contacts between each rock type at outcrops along stream networks within each study watershed.

Early Proterozoic gneiss occurs at lowest elevations, along the Main Stem stream and at the outlets of the sub watersheds. The gneiss is medium to coarsely crystalline hornblende biotite gneiss with interspersed

dikes of pink orthoclase feldspar with plagioclase feldspar and quartz, parallel to the gneissic foliation [*Reynolds*, 1995]. The Gneiss fractures in blocks and forms cliffs, present along the Main Stem and lower Bubbling creeks. There is limited potential for water movement in this unit through irregular fractures and open vugs in quartz-rich laminae [*Reynolds*, 1995].

Flathead Sandstone overlays the Gneiss at middle watershed elevations, which is a fine to coarse grained sandstone cemented with quartz. The sandstone is interbedded with a sandy siltstone several centimeters thick, increasing in quantity at the top of the unit. It is firmly cemented, forms steep slopes, and has low permeability. However, the top of this unit is uniformly fractured and is likely the primary location for groundwater movement and storage in the watershed [*Reynolds*, 1995].

Middle Cambrian Wolsey shale rests on top of the Flathead sandstone at higher elevations. The Wolsey shale is made up of predominantly gray and greenish gray clayey siltstone, claystone, and sandy siltstone lower in the unit. The rock has low permeability but is very fractured, typically platy, characteristic of shale [*Reynolds*, 1995]. Parks over this unit generally become saturated with water in the spring, which then percolates down and reemerges as seeps and springs along the contact with the sandstone. The seeps and springs are often located near the stream initiation points in the watersheds [*Payn et al*., 2012].

3. Methods

3.1. Stage Measurements

The TCEF is equipped with flumes located at the outlet of each subwatershed with additional flumes located midway in the Stringer and Main Stem watersheds (H-Flumes: Stringer, middle Stringer, Bubbling; Parshall Flumes: Sun, Spring Park, Lower Tenderfoot, and upper Tenderfoot). All flumes continuously record hourly water levels in stilling wells connected to the flumes [*Farnes and McCaughey*, 1995]. We augmented the existing streamflow monitoring network by installing 43 in-stream stilling wells at ~250 m valley distances in the Main Stem, Stringer, Spring Park, Sun, and Bubbling subwatersheds (Figure 1). Stream locations for each stilling well were chosen at locations that would show an appreciable increase in stage with discharge and where the channel geometry was deemed to be stable through time [*Sauer and Turnipseed*, 2010]. Stilling wells consisted of a fence post driven in to the stream bottom, with a 2 inch diameter screened section of pvc pipe attached and resting on the channel bottom. Within the stilling well, capacitance rods (TruTrack Inc., Christchurch, NZ) were installed to measure hourly water levels and water temperature ($\pm$1 mm accuracy). Capacitance rods were deployed in the field from 10 May to 30 September 2013 and downloaded at bi-weekly intervals.

3.2. Discharge Calculations

We used the dilution gaging method to measure an instantaneous discharge at each stilling well and USFS flume [*Day*, 1976]. Dilution gauging is a widely accepted method of measuring streamflow and works particularly well in small, high-gradient streams with irregular stream bottoms such as the TCEF [*Day*, 1976; *Zellweger et al*., 1989]. It involves instantaneously injecting a known quantity of conservative tracer (in this case NaCl in solution) above a measurement point [*Covino et al*., 2011]. The injected salt fully mixes in the water column along a short mixing length, the distance between the injection point and the measurement point. Along the short mixing length, it is assumed that discharge is constant and no tracer is lost [*Kilpatrick and Cobb*, 1985]. An electrical conductivity probe with data logger was placed in the thalweg at the measurement point to measure the specific conductivity (SC) breakthrough curve (Campbell CR1000 data logger and CS-547A temperature/conductivity probe, Campbell Scientific, Inc., Logan, UT, USA).

Each dilution gauging measurement results in a recorded breakthrough curve of the increase in SC as the dissolved NaCl moves past the measurement point. We integrated under the breakthrough curve to calculate the total increase in SC and then used a known relationship between SC and Cl^- to calculate a volume of water or discharge (equation (1)) [*Covino et al*., 2011]:

$$Q = \frac{T_{MA}}{\int_0^t T_c(t)dt}, \tag{1}$$

where Q is discharge, T_{MA} is the tracer (NaCl) mass added, and T_C is the background corrected tracer concentration. To evaluate the precision of our dilution gauging measurements we performed 42 replicate

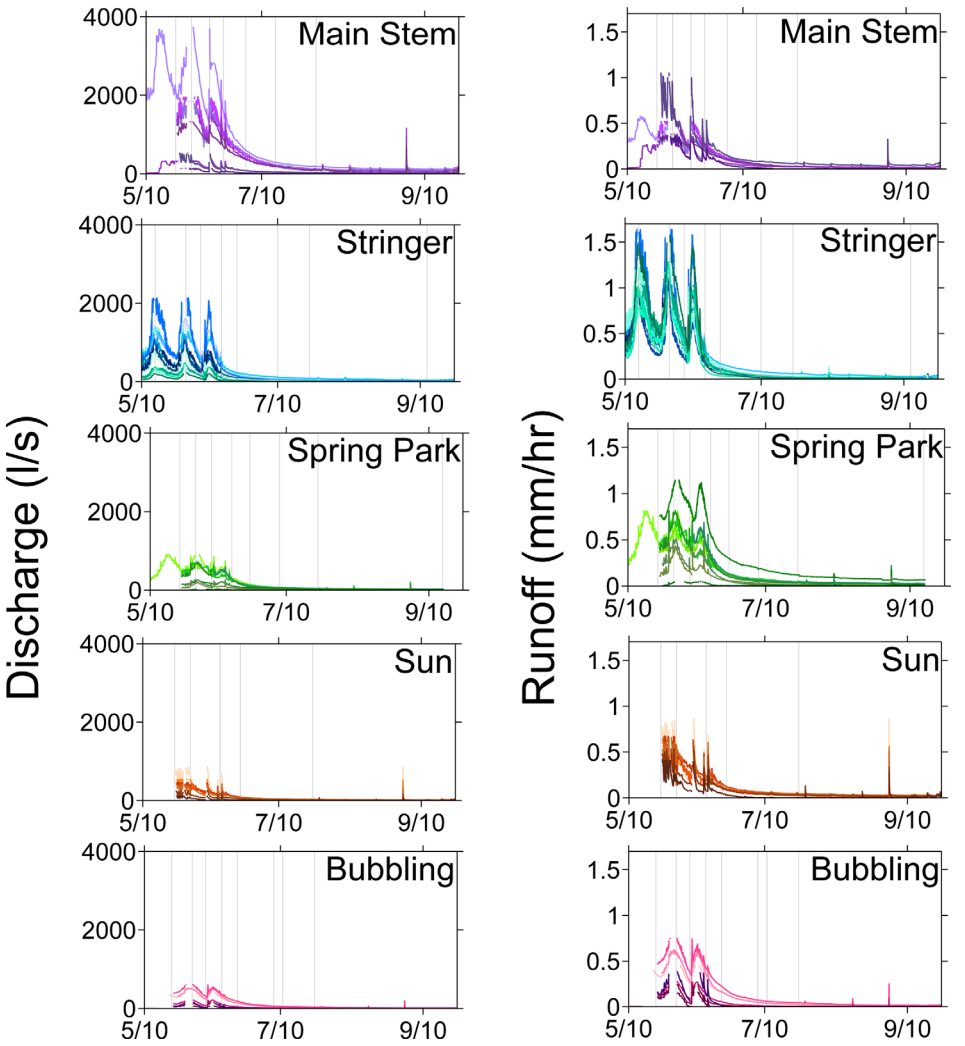

Figure 2. Hydrographs of each stilling well within the TCEF subwatersheds during the 2013 season. The left column depicts absolute discharge and the right column depicts area normalized discharge. Gray lines behind each hydrograph indicate times at which direct measurements of discharge were completed. Subwatersheds from top to bottom include: the Main Stem of Tenderfoot Creek, Stringer Creek, Spring Park, Sun Creek, and Bubbling. Lights shades in each watershed indicate measurement points closer to the watershed outlet.

dilution gauging discharge measurements across several flow states throughout the season. Replicates were a second dilution gauging measurement at the same location after the initial dilution gauging experiment was performed; the second slug was introduced 15 min after the stream returned to background. The average precision was 1.5% of discharge with a maximum replication error of 9.6% and a minimum error of 0.02% of measured discharge.

3.3. Stage–Discharge Rating Curves

Dilution gauging was performed as many times as possible at each stilling well in order to build a stage-discharge rating curve for each stilling well and verify rating curves at the USFS flumes (6–12 measurements at each location across the annual hydrograph). Discharge measurements were performed most frequently during snowmelt and recession and at reduced frequency at low flow because discharge was not changing as rapidly (Figure 2). During each dilution gauging measurement, stage was manually measured to verify the recorded stage at each capacitance rod. For each stilling well, we performed regression analyses between the measured discharge values and observed stages across the full range of flow states. All of the resulting rating curves exhibited significant power law relationships (R^2 range: 0.94–0.98). We applied each regression equation to the recorded hourly stage data to calculate hourly discharge at each stilling well from 10 May to 30 September 2013 (Figure 2, left). To avoid error, no calculated discharge data were used

for our analysis if it was above the highest manually measured discharge. Because we were able to perform dilution gauging close to peak snowmelt, very little data were omitted (a maximum of five consecutive days). Hourly time series were normalized by contributing area to compare differences in runoff between locations within and across subwatersheds (Figure 2, right). We also used hourly time series to calculate weekly and daily average discharges at each stilling well in order to examine discharge trends through time.

3.4. Mass Recovery

In addition to measuring discharge, we used the mass recovery method [*Harvey and Bencala*, 1993; *Harvey et al*., 1996; *Triska et al*., 1989] to measure gross hydrologic gains and losses along stream reaches in the Stringer Creek watershed. We define a stream reach as the stream section between two gauging locations, which is distinct from and much longer than a mixing length defined above. A gross gain is the total amount of water that entered over the stream reach, and a gross loss is the total amount of water that left the stream channel over that reach. The balance of the two is the net discharge. A net discharge can be determined from calculating the difference in discharge from the top and bottom of a reach, however it does not provide any information on the gross exchange or gain and loss of water [*Covino and McGlynn*, 2007; *Payn et al*., 2009; *Covino et al*., 2011].

First we measured discharge at the top and bottom of a reach using the dilution gauging method to determine the net discharge of the reach (ΔQ, *net Q*). Then, at the top of the reach a greater mass of NaCl was injected and the breakthrough curve of the injection was measured at the base of the reach. Along the reach, water enters (diluting the NaCl) and exits the channel (with its associated NaCl), thus not all of the NaCl mass would be observed at the bottom of the reach.

The breakthrough curve at the base of the reach is directly related to the proportion of salt recovered at the base of the reach (equation (2)) [*Covino et al*., 2011]. The mass of tracer lost (M_{lost}) was calculated by subtracting the tracer mass recovered at the bottom of the study reach (M_{rec}) from the tracer mass added at the top of the reach (M_{top}) where Q is discharge at the base of the reach:

$$M_{lost} = M_{top} - M_{rec} = M_{top} - Q \int_0^t T_c(t)dt. \quad (2)$$

The discharge lost (Q_{lost}) in each reach was calculated as the product of the percent of tracer mass lost by the average discharge in the reach. Using an average discharge assumes concurrent gain and loss within a reach [*Payn et al*., 2009; *Exner-Kittridge et al*., 2014].

Discharge gained was then calculated through mass balance:

$$Q_{gain} = \Delta Q + Q_{lost}. \quad (3)$$

Gross gains and losses were normalized by 100 m of stream length to facilitate comparison across uneven length reaches. We performed four sets of mass recovery experiments in the Stringer Creek watershed during the 2013 field season across 14 stream reaches: 20 June, 27 June, 15 July, and 20 September. Discharge at the outlet of the watershed at these times was 494, 207, 70, and 27 L/s, respectively.

3.5. Spatial Analyses of Discharge and Exchange

We sought to understand how spatial and temporal dynamics in stream discharge related to variability in watershed structure both at large watershed scales and across increasingly smaller subwatershed sizes. To do so, we calculated watershed contributing areas from the reach to watershed scale using 10 m light detection and ranging (LiDAR) derived digital elevation model (DEM). Additionally, we calculated a number of terrain metrics using the DEM, geologic mapping by *Reynolds* [1995], vegetation characteristics derived from LiDAR returns, and optical and field survey data of the TCEF stream morphology.

We calculated the contributing area to each gauging location and flume using a unidirectional flow direction algorithm (D-8) [*O'Callaghan and Mark*, 1984]. The topographically based contributing areas were separated in two ways: total contributing area, which is the entire watershed area contributing water to the gauging location (all area upstream of that point), and lateral contributing area, which we define as the hillslope area contributing water specifically to the stream reach (between the gauging location and the next upstream gauging location). We define a watershed as one of each of the five watersheds that compose the

Table 1. The Predictor Variables Used in Stepwise Multiple Linear Regression Analyses With Observations of Stream Gross Gains in the Stringer Creek Watershed[a]

Reach Number	Dominant Geology	Lateral Contributing Area (km^2)	Median Slope (radians)	Median DFC (m)	Median GTC	Median Insolation (w/m^2 yr)	Median Tree Density	Riparian Area (m^2)	Median Elevation (m)
1	Gneiss	0.23	0.17	266.07	0.34	3406.41	0.24	6,300	2,123
2	Gneiss	0.19	0.15	280.22	0.32	3421.40	0.31	3,600	2,135
3	Gneiss	0.13	0.22	266.07	0.26	3359.41	0.32	2,800	2,132
4	Gneiss	0.24	0.18	260.31	0.26	3476.08	0.31	6,200	2,149
5	Gneiss	0.80	0.15	402.09	0.14	3484.92	0.31	10,100	2,208
6	Sandstone	0.11	0.23	216.89	0.25	3406.91	0.39	3,000	2,156
7	Sandstone	0.19	0.17	306.47	0.19	3421.68	0.34	3,500	2,176
8	Sandstone	0.32	0.13	409.42	0.17	3483.93	0.31	4,600	2,198
9	Sandstone	0.28	0.15	308.41	0.18	3447.46	0.35	7,300	2,198
10	Sandstone	0.51	0.18	512.72	0.15	3426.12	0.31	8,200	2,244
11	Sandstone	1.03	0.09	472.65	0.08	3478.50	0.30	16,100	2,227
12	Sandstone	0.09	0.19	244.13	0.16	3425.15	0.40	4,200	2,213
13	Sandstone	0.13	0.19	376.21	0.14	3415.44	0.38	2,700	2,239
14	Sandstone	0.73	0.16	555.11	0.14	3432.08	0.28	6,400	2,274

[a]DFC is distance from creek and GTC is the gradient to creek.

TCEF: Main Stem, Stringer, Spring Park, Sun, and Bubbling. A subwatershed is the progressive division of each watershed at the stilling wells located within it; the total contributing area draining to each stilling well. The lateral contributing area is the area contributing only to the stream reach between gauging locations as defined earlier in this paragraph. For each lateral contributing area, we derived 14 distributed topographic indices that represent water redistribution and exchange (Tables 1 and 2).

Measures of the channel structure were performed with optical surveys and visual assessments of the dominant stream reach morphology from the outlet to the channel initiation (R. Payn and K. G. Jencso, Stream channel survey of Stringer Creek, unpublished data). Benchmarks were installed using survey grade GPS (Trimble 5700, 5 mm horizontal and vertical accuracy) and control points along the stream network. From those points, optical surveys were performed for the channel and transitions between unique stream geomorphic features that included riffles, runs, pools, steps, and cascades [*Montgomery and Buffington*, 1997]. Streambed elevations at the beginning and end of each feature were also recorded. We digitized and categorized the survey data by the geomorphic features listed above, where each feature had information on the location, elevation loss, and the stream length over which it was observed. Across each reach, counts of the number of features by geomorphic type were also recorded. Because the reaches were not uniform in length we normalized the feature count per 100 m of stream in order to make comparisons across the reaches. These survey data were used to calculate all metrics except dominant geology in Table 2.

Table 2. The Predictor Variables Used in Stepwise Multiple Linear Regression Analyses With Observations of Stream Gross Losses in the Stringer Creek Watershed

Reach Number	Reach Geology	Nonnormalized Step Count	Normalized Step Count	Normalized Elevation Loss (m)	Median Channel Slope	Standard Deviation of Channel Slope
1	Gneiss	33	9.64	0.0473	0.0942	0.12
2	Gneiss	21	8.66	0.0305	0.0863	0.16
3	Gneiss	12	8.05	0.0384	0.1148	0.18
4	Gneiss	31	8.26	0.0408	0.1152	0.18
5	Gneiss	15	7.90	0.0395	0.1007	0.19
6	Sandstone	10	3.25	0.0110	0.0953	0.18
7	Sandstone	17	4.98	0.0185	0.1021	0.15
8	Sandstone	10	3.96	0.0117	0.0718	0.11
9	Sandstone	5	1.46	0.0053	0.0623	0.10
10	Sandstone	8	2.86	0.0075	0.0520	0.11
11	Sandstone	19	4.17	0.0090	0.0624	0.11
12	Sandstone	6	0.90	0.0021	0.0649	0.12
13	Sandstone	8	2.82	0.0095	0.0611	0.13
14	Sandstone	8	2.16	0.0058	0.0564	0.12

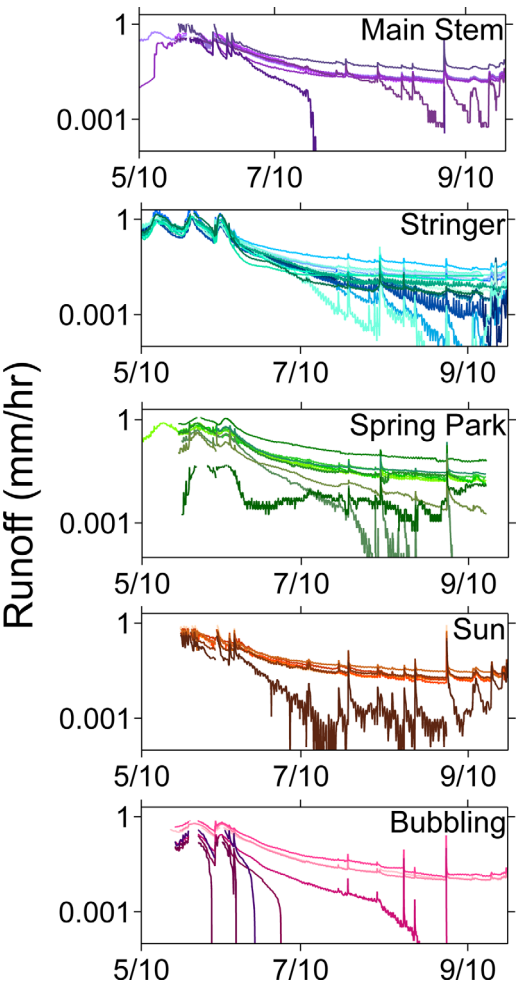

Figure 3. Runoff time series of each stilling well in the 2013 season by subwatershed: Main Stem, Stringer, Spring Park, Sun, and Bubbling from top to bottom. Lighter shades indicate points closer to the watershed outlet. Note logged *y* axis. There is at least an order of magnitude difference in area normalized discharge across stilling wells for each subwatershed during high flow, which increases toward low flow. Headwater stilling wells in the Main Stem and Bubbling watersheds are ephemeral.

At the scale of the TCEF watersheds we used correlation analysis to evaluate the relationships between weekly and daily averages of total discharge, as well as the net discharge with total contributing area and each of the lateral contributing areas, respectively. We also implemented stepwise multiple regression analysis to test how incremental changes in gross gains and losses within the Stringer Creek watershed related to 15 indices that have been shown to influence runoff generation and streamflow (Tables 1 and 2). The stepwise multiple regression analysis between these values and the gross gains and losses for each reach were performed in the statistical program R. Model goodness of fit for each combination of variables was assessed using Akaike's information criterion (AIC). The predictors were dropped or added according to a respective increase or decrease in the AIC for each modeled time period. The predictors selected for each regression equation were those that were significant ($P < 0.05$) for explaining the differences in gains and losses across the Stringer Creek reaches.

4. Results

4.1. Discharge Time Series

In general, stream discharge (Q) increased with watershed area within and across each of the TCEF watersheds (Figure 2). If increasing contributing area explained all of the variability in discharge, then runoff (discharge normalized by area) should be similar at each of our monitoring locations. However, certain watersheds and subwatersheds produced more streamflow per unit area than others (Figure 2, right). The Stringer watershed had the highest runoff, peak flow values were ~1.4 mm/h; Bubbling and Sun had the lowest around 0.8 mm/h. Within both the Stringer and Sun watersheds, gauging locations had more similar runoff during high flow: all areas in those watersheds yielded a similar amount of streamflow per unit area (range of 0.27 mm/h in Sun and 0.33 mm/h in Stringer). There was more variability in runoff within the Spring Park and Bubbling watersheds (range of 0.69 mm/h in Spring Park and 0.56 mm/h in Bubbling). During low flow periods (Figure 3), there was an even larger difference in runoff between the gauging locations and the degree of divergence increased as the season progressed. We observed several orders of magnitude difference in discharge per unit area at low flow both within and across watersheds. In addition, some of the gauging locations had extremely low runoff values by the end of season relative to other locations with similar contributing area. These were frequently the gauging locations closest to channel initiation, particularly in the Spring Park and Sun watersheds (Figures 3c and 3d, respectively). We also observed ephemeral flow at the headwaters of two watersheds: the Main Stem and Bubbling (Figures 3a and 3e, respectively). In the Main Stem, the channel network contracted below the uppermost gauging location beginning on 20 July. In Bubbling, there was no streamflow at the three uppermost gauging locations by 6 June. The next downstream gauging location in Bubbling had continuous flow throughout the year, but it was too low (<1 L/s) to accurately measure by the first week of August.

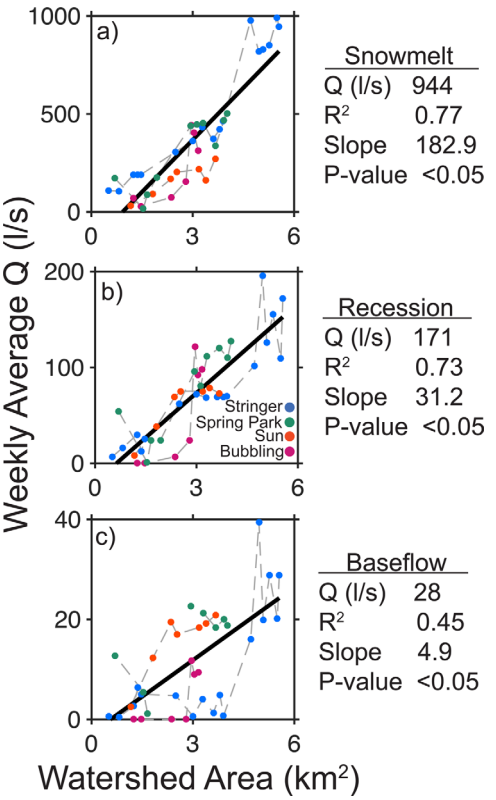

Figure 4. Linear regressions between total watershed contributing area and weekly average discharge at (a) peak snowmelt, (b) recession, and (c) base flow in the 2013 season with all stilling wells in the Stringer, Bubbling, Spring Park, and Sun watersheds combined. The regressions indicate decreased yield over time (decreasing slope) and increased variance in the discharge-area relationship. Dashed gray lines show the differences in discharge accumulation with watershed area across each of the subwatersheds.

4.2. Discharge Variability at the Watershed and Subwatershed Scales

We performed linear regression between total contributing area and a weekly average *Q* for all of the gauging locations in Stringer, Spring Park, Sun, and Bubbling at three contrasting flow states and found significant, positive relationships (Figure 4). Here, we used a weekly average discharge in order to capture a general behavior of each flow state: peak snowmelt (Figure 4a, 944 L/s), recession (Figure 4b, 171 L/s), and late season base flow (Figure 4c, 28 L/s). All streams in the TCEF generally increase in discharge moving downstream, therefore this relationship was necessarily positive because it is derived from absolute discharge and total contributing area to each point and incorporates the discharge and contributing area of every point upstream (i.e., aggregate watershed behavior).

The slope of the relationship between total watershed area and weekly average Q declined with declining flow states; there was less *Q* per unit area (Figure 4). Additionally, the goodness of fit of the contributing area–*Q* relationship decreased through flow states from an R^2 of 0.77 at snowmelt to 0.45 by base flow (Figure 4). Across all of the flow states there was scatter about the linear relationship and this became more pronounced toward the base flow time period. By the low flow period, many gauging locations had very little *Q*, even with contributing areas close to 4 km^2 (Figure 4). We also observed different rates at which discharge increased with total contributing area within and across the subwatersheds (Figure 4; dashed lines for each subwatershed).

4.3. Scaling of the Contributing Area Discharge Relationship

Our preliminary results indicated a high degree of variability in yield across subwatersheds and time periods. To evaluate this behavior across multiple nested scales we used a stepwise aggregation of lateral contributing area (area contributing directly to the gauging location) and the net discharge (the net amount of water that entered or left between the upstream and downstream gauging locations). This illustrates how the relationship between lateral contributing area and net discharge progresses from high to low flow states and from large to small spatial scales (Figure 5).

The relationships between lateral contributing area and change in *Q* were only significant at the watershed scale (Figure 5a) and when the watersheds were divided in half during high flow (Figure 5b, top). We began to observe negative changes in discharge at the half watershed scale (Figure 5b). At a given flow state, smaller areas generally resulted in less inflows to the channel (Figure 5, left to right in a row). However, across the smallest divisions of lateral contributing area (Figure 5d) we also observed negative changes in discharge. A negative change in discharge indicated that there was substantial loss of water across a reach that exceeded the water entering the reach from the adjacent hillslopes.

4.4. Reach Scale Water Balance

Generally, we observed more exchange (the balance of gross gains and losses) closer to the outlet (Figure 6, reaches 1–5) relative to the upstream reaches (Figure 6, reaches 6–14). This pattern was consistent across flow states, but the absolute volume of exchange decreased over the course of the snowmelt recession. Additionally, most reaches were consistently net gaining or losing with one exception being reach 12,

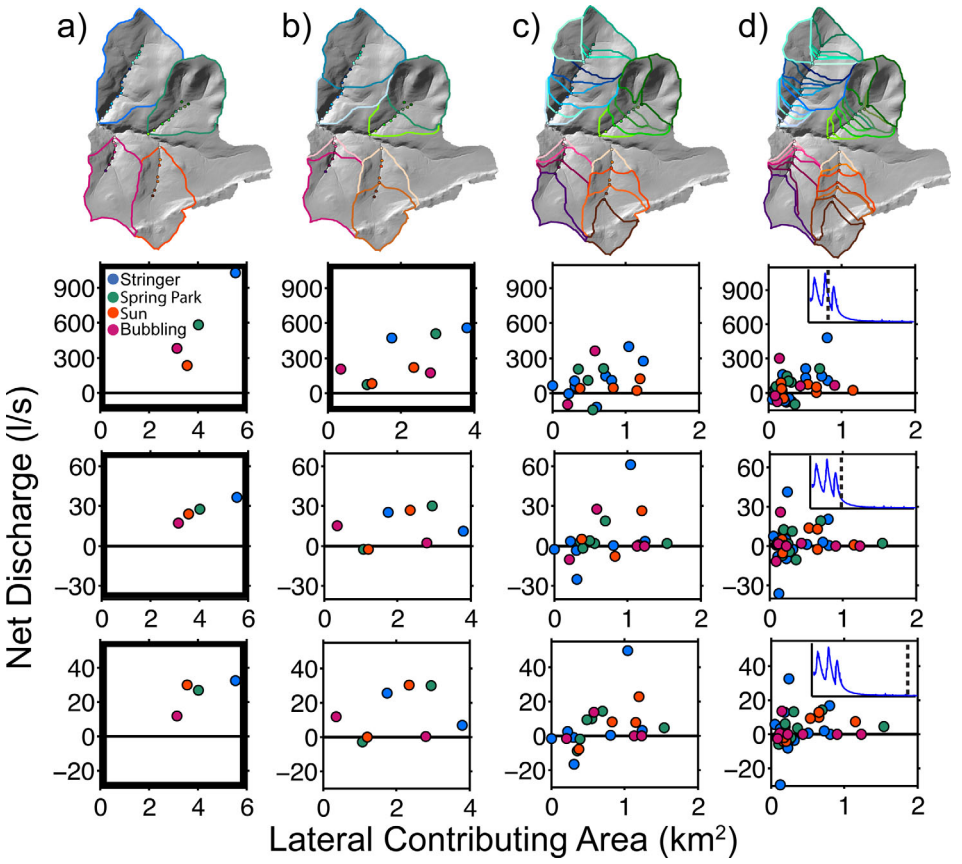

Figure 5. The relationship between lateral contributing area and net in discharge across spatial scales and flow states. Flow states progress from snowmelt in the top row, recession in the middle row, and base flow on the bottom row, indicated by hydrographs in Figure 5d. Flow states are the same as those presented in Figure 4. Spatial scales progress from large (left) to small lateral contributing areas (right); (a) subwatersheds of the TCEF, (b) subwatersheds divided in half, (c) two stilling wells combined, and (d) individual stilling wells. In Figure 5a, net discharge is simply outlet discharge. In subsequent panels, net discharge is the difference between upstream discharge and discharge at the subwatershed "outlet." Plots with bold outlines have significant relationships between lateral contributing area and the change in discharge. There is only a significant relationship between lateral contributing area and change in discharge at the subwatershed scale (a) and the subwatersheds divided in half at highest flow (b, top row). More negative changes in discharge are observed at increasingly smaller scales (b–d).

which was strongly losing during the highest flow (Figure 6a) but strongly gaining at all other measurement times (Figures 6b–6d).

Stepwise multiple regression analysis indicated that increases in the reach lateral contributing area and the dominant underlying lithology type were the only significant predictors of the volume of gross gains across the channel network (Table 3; $R^2 = 0.70–0.85$, $P = <0.01–0.049$) for the first three flow periods following snowmelt (494, 207, and 70 L/s). During the lowest flow period in fall (September) the addition of vegetation density with lateral area and stream reach lithology explained 87% of the variance in stream gross gains (Table 3). Increased vegetation densities were associated with greater gross gains and an additional 18% increase in the variance explained, relative to a regression model with only lateral area and lithology. Importantly, the coefficient for vegetation density, the change in gross gain with 1 unit increase in density if contributing area and rock type are held constant, was positive (38.25).

The relationships between contributing area and gains separated by dominant rock type were particularly strong for sandstone dominated reaches at higher flows: $R^2 = 0.84$ and 0.89 (Figures 7a and 7b, respectively). By late season base flow, very little water was contributed to streams from the reaches underlain by sandstone, the slope of this relationship was only 1.3 L/s per km^2 (Figure 7d). The slope of each relationship for both groups of reaches decreased with lower flow states: 126.1–17.7 L/s per km^2 in gneiss and 77.9–1.3 L/s per km^2 in sandstone (Figure 7). The slope of the regression for gneiss dominated reaches was always much higher than sandstone dominated reaches.

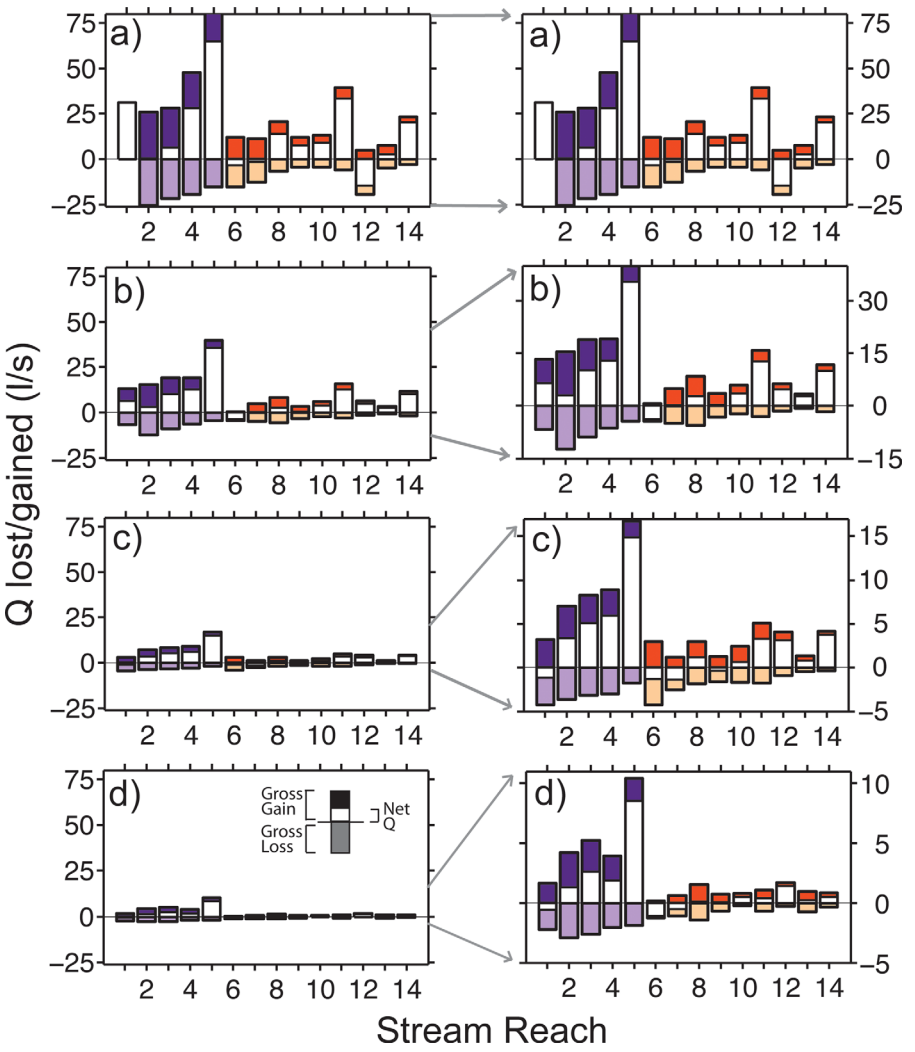

Figure 6. Gross gains (positive bars) and gross losses (negative bars) per 100 m across consecutive stream reaches in the Stringer watershed for the 2013 season. White bars are the net discharge that result from the gross gain and loss within each reach. Bar colors are representative of the dominant underlying lithology of the reach, purple is gneiss while orange is sandstone. Reaches with lower numbers are closer to the outlet. Measurements were made at (a) 6/20, 494 L/s outlet *Q*; (b) 6/27, 207 L/s outlet *Q*; (c) 7/15, 70 L/s outlet *Q*; (d) 9/20, 27 L/s outlet *Q*. The left column is on a fixed *y* scale and the right column is the same data but scaled to the maximum gain/loss of each measurement time period.

The normalized count of steps across each reach was the only significant predictor of gross loss across all flow states (Figure 8). These relationships were significant at the 0.05 alpha level except at the 70 L/s flow state, which was significant at the 0.01 alpha level with an R^2 of 0.43. The slope of the relationship declined

Table 3. Results From Stepwise Multiple Linear Models of Landscape Structure and Stream Gross Gains[a]

Flow Period (L/s)	Adjusted Multiple r^2	Intercept	Lateral Area	Lithology	Tree Density
494	0.70	120.78	90.78	−60.07	–
		<0.01	*<0.01*	*<0.01*	
207	0.85	60.87	42.12	−31.29	–
		<0.01	*<0.01*	*<0.01*	
70	0.69	25.76	13.85	−12.68	–
		<0.01	<0.01	<0.01	
27	0.86	3.6	3.42	−11.00	38.25
		<0.01	*0.049*	*<0.01*	*<0.01*

[a]Each model is listed in order of decreasing streamflow. Regression coefficients are listed with their associated *P* value (italics). A missing value indicates that the predictor was not retained in the final model. Variables that were not found to be significant (Table 1) during any time period were omitted.

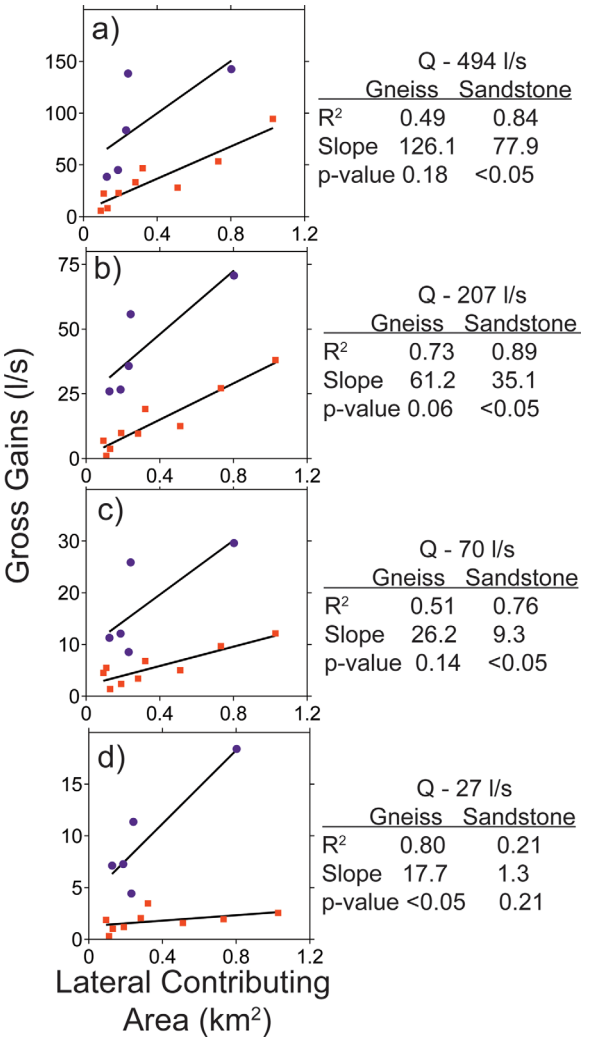

Figure 7. Linear regressions between lateral contributing area and gross hydrologic gains classified by dominant lithology (purple: gneiss, orange: sandstone) at four time periods across the 2013 water year: 6/20, 6/27, 7/15 and 9/20. Gneiss dominated reaches consistently yield more water than those dominated by sandstone lithology. Gross gains decrease with decreasing flow state across all reaches, however lateral contributing area remains a significant predictor of gross gains at all measurement periods.

with reduced flow states (from 4.21 to 0.58 L/s per step). Regressions were performed with all reaches, not separated by dominant geology. We combined the normalized step and cascade feature counts from the Stringer creek survey data (hereafter collectively referred to as steps) because both types have abrupt head drops [*Montgomery and Buffington*, 1997]. There were more steps per stream length lower in the watershed in locations where gneiss was present. In addition, the total elevation change associated with these features in each reach was greater closer to the outlet (Figure 8, symbol size). However, this did not improve predictions of gross loss in a reach. For example, the largest gross loss in the second mass recovery experiment was in a reach with less total elevation loss than the next two largest volumetric gross losses (Figure 8b).

5. Discussion

In this study, we aimed to identify the dominant watershed properties that influence the timing and magnitude of stream flow and how this scales from the reach to the entire watershed. Common elements that have been shown to influence spatiotemporal variability in streamflow include topographic characteristics such as contributing area [e.g., *Anderson and Burt*, 1978; *Beven and Kirkby*, 1979; *Wood et al.*, 1988; *Jencso et al.*, 2009], vegetation [*Rodriguez-Iturbe and Porporato*, 2004; *Nippgen et al.*, 2015], subsurface characteristics such as bedrock structure [e.g., *Huff et al.*, 1982; *Freer et al.*, 2002; *Uchida et al.*, 2005], and differences in valley bottom–stream geomorphology [*Harvey and Bencala*, 1993; *Ward et al.*, 2012; *Wondzell*, 2006] that can promote bi-directional exchanges (gains and losses) of water between streams and valley bottom systems. However, we have not yet resolved how channel and valley hydrologic exchange can modulate hillslope contributions to streams or how this leads to differences in watershed scale discharge dynamics.

At the scale of large watersheds, a common approach to account for spatial and temporal variability of contributions to streamflow has been to further divide subwatersheds into topographically based contributing areas. Previous work has highlighted the challenge of scaling discharge with contributing area and difficulties in transferring these relationships to alternative basins with different climate, topography, lithology, and vegetation characteristics [e.g., *Wood et al.*, 1988; *Smith*, 1992; *Gupta et al.*, 1996, 1994; *Seyfried and Wilcox*, 1995; *Wood et al.*, 1988; *Eaton et al.*, 2002; *Yue and Gan*, 2009]. Across the TCEF watersheds, there were significant and positive linear relationships between total watershed contributing area and total discharge that weakened over the course of the seasonal hydrograph recession (Figure 4). This was expected since the compound effect of inflows from all upstream contributing area in conjunction with those associated with new lateral area contributing directly to the reach result in a positive relationship.

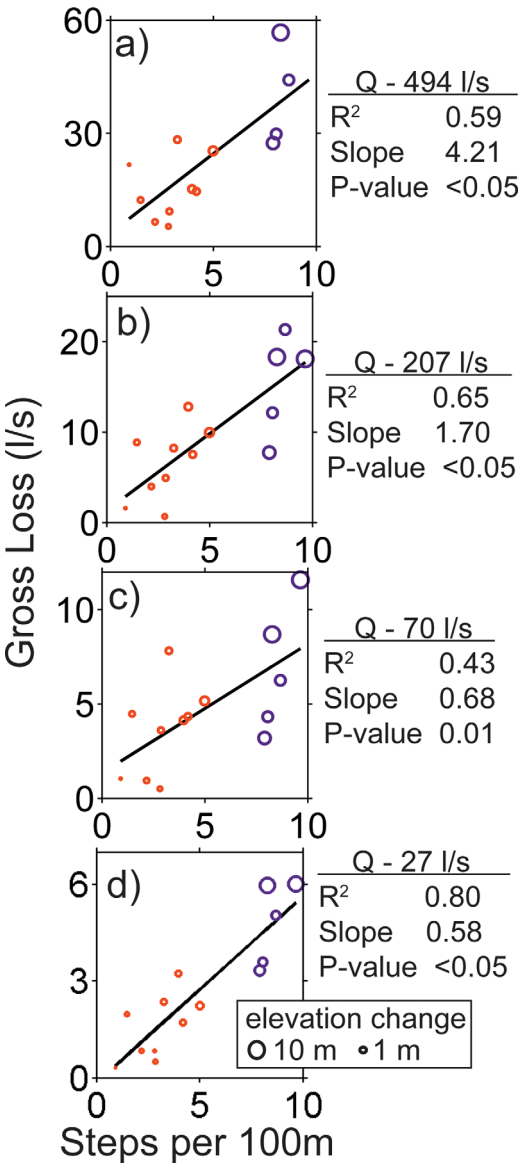

Figure 8. The linear relationship between gross losses and a count of the number of steps in each reach (normalized per 100 m) derived from survey data in the Stringer Creek watershed (orange: sandstone dominated reaches, purple: gneiss dominated reaches). Losses were calculated from mass recovery experiments performed across flow states in the 2013 water year on 6/20, 6/27, 7/15, and 9/20. This suggests that stream morphology controls volumetric gross losses once water enters the stream network. Each symbol size is scaled by the sum of elevation lost over all steps in the reach.

In order to better isolate spatiotemporal variability in the contributions to streamflow, we progressively subdivided watershed contributing area and quantified the relationship between contributing area and net discharge, an approach that has previously been used at both large [e.g., *Eaton et al*., 2002; *Yue and Gan*, 2009] and small scales [e.g., *Wood et al*., 1988]. We found that the relationship between net discharge and contributing area is only significant at scales of 1.5 km^2 and larger (Figure 5), which is consistent with the findings of *Wood et al*. [1988]. At scales smaller than this we observe negative changes in discharge suggesting substantial loss of flow from the stream reach (Figures 5b–5d). Even some of the aggregated stream reaches (~1 km long, 1.5 km^2 contributing area) lost more water from the channel network than was gained from the lateral contributing areas (resulting in a negative change in discharge). These contributing areas may have intersected longer, more intermediate flow paths in the valley system [*Toth*, 1963], whereby water that was lost from a stream reach returned further downstream. For example, *Payn et al*. [2012] concluded that losses from upstream reaches traveling along intermediate flow paths reemerge downstream and contribute to more discharge than expected from the downstream lateral areas. Additionally, the influence of hydrologic exchange between the stream and valley groundwater system on net discharge may also increase as flow state decreases; we observed proportionally more negative changes in discharge with decreasing flow states and subwatershed sizes (Figures 5b–5d). This highlights the need to consider how variability in hillslope contributions and channel losses to the valley groundwater system may contribute to aggregate discharge dynamics.

5.1. How Does Upland and Stream Structure Lead to Differences in the Gross Channel Water Balance and Cumulative Discharge Dynamics?

5.1.1. Combined Topographic and Geologic Controls on Stream Reach Gross Gains

The significant and positive linear relationships between gross gains of water and lateral contributing area highlight the importance of considering the channel water balance when quantifying the potential for hillslope contributions to stream discharge (i.e., gross gains versus net increase in discharge). Hillslope contributions to peak runoff in the TCEF are dominated by shallow subsurface flow that is strongly topographically controlled [*Jencso et al*., 2009]. During snowmelt, soils become saturated and there was development of a shallow subsurface water table connecting all but the smallest hillslopes to adjacent valley bottoms and stream reaches [*Jencso et al*., 2009; *Nippgen et al*., 2015]. This is reflected in the strong relationship and steep slope between lateral contributing area and gross gains at this time period (Figure 7a). During the recession from peak snowmelt runoff and decreasing overall watershed moisture state, hillslopes with smaller contributing areas become hydrologically disconnected and the slope of the relationship

between discharge and contributing area began to decrease (Figures 7b and 7c). By late season (low base flow), modeling by *Smith et al*. [2013] estimated that only approximately 5% of the stream network was hydrologically connected to the uplands via shallow subsurface flow. Very little water per unit contributing area was being delivered to the stream network (Figure 7d). During this time period, reach characteristics such as individual large contributing areas (large convergent hillslopes that have continuous hydrologic connectivity) may become more influential on spatial patterns of discharge gains [*Anderson and Burt*, 1978; *Jencso et al*., 2010; *Smith et al*., 2013; *Nippgen et al*., 2015].

The dominant underlying lithology was also an important consideration for the magnitude of gross gain to each stream reach, as previously suggested by *Payn et al*. [2012]. Two different relationships were apparent depending on whether the lower portions of each reach lateral contributing area was underlain by gneiss or sandstone (Figure 7). Areas underlain by sandstone yielded much less water than those underlain by gneiss. The largest disparity between yields from areas with different rock types was late in the season. In the sandstone there was almost no increase in gross gain with increase in contributing area (slope 1.3 L/s km^2, Figure 7d). This suggested that hillslopes underlain by sandstone were contributing little to no water to streamflow late in the season.

There are numerous plausible explanations for the differences in stream gains associated with lateral contributing areas across the different geologic settings. For example, differences in the permeability of each rock type may have influenced the partitioning of water between deep and shallow groundwater flow paths that eventually become stream flow [*Graham et al*., 2010; *Jencso and McGlynn*, 2011; *Gabrielli et al*., 2012; *Payn et al*., 2012; *Creutzfeldt et al*., 2014]. In this case, decreased yields in areas underlain by sandstone (Figure 7) may be related to the permeability of the sandstone unit, which is higher than the gneiss due to grain size distributions, the nature of the cementation, and a regular fracture network at the surface [*Reynolds*, 1995]. In addition, *Payn et al*. [2012] concluded that in Stringer, when water moving within the sandstone encounters the relatively impermeable gneiss at lithological transitions, it will likely emerge again in the shallow subsurface as seeps or springs or directly as streamflow (e.g., Figure 6, reach 5). It is also possible that differences in soil hydraulic conductivity could exist across the sandstone and gneiss parent material. This could contribute to order of magnitude differences in water fluxes to downslope locations during time periods of unsaturated flow (throughflow) and transitions to saturated soil wetness states (subsurface flow) [*Soulsby et al*., 2004, 2006; *Tromp-van Meerveld and McDonnell*, 2006; *Tetzlaff et al*., 2014; *Gannon et al*., 2014]. Without additional lines of inference (e.g., isotopic or chemical tracers, deep groundwater wells, and geophysical measurements), it is difficult to separate the relative contributions from the shallow subsurface and deeper geologic flow paths that converge within the valley bottoms.

Previous analysis across 15 of the 24 shallow groundwater transects in the TCEF suggested that increased vegetation densities contributed to higher magnitude transpiration and decreases in annual hydrologic connectivity along hillslope flow paths [*Emanuel et al*., 2013]. However, our multiple linear regression analysis indicated that increased vegetation density was associated with stream gains, but only during the lowest flow period. These contrasting results may highlight the role of vegetation for seasonal differences in the partitioning of evaporation and transpiration across upslope flow paths. For example, decreases in soil water potential during the drier time period could have contributed to decreased transpiration through stomatal closure [*Rodriguez-Iturbe and Porporato*, 2004; *Porporato et al*., 2004; *Emanuel et al*., 2010]. At the same time, the increased leaf area associated with dense forest stands may have reduced soil water evaporation through shading of incoming radiation and resulted in concomitant increases in throughflow downslope. It should be noted that 7 of the 24 hillslope well transects in the *Emanuel et al*. [2013] study did not follow the overall trend and indicated greater durations of hydrologic connectivity with increasing tree density. It was suggested that increased upslope contributing area and bedrock seeps at some transects (the seven that did not follow the global relationship) may have contributed to more plant available water and higher vegetation densities along upslope flow paths.

Previous hillslope scale and theoretical studies in the TCEF have also suggested the influence of alternative factors. These have included variability in snowpack melt timing and magnitudes that influence recharge to the shallow subsurface [*Smith et al*., 2013] and differences in hillslope flow path gradients that led to differences in the rate of water delivery to the stream network [*Jencso and McGlynn*, 2011; *Nippgen et al*., 2015]. In this study these additional factors resulted in decreased model parsimony without a significant increase

in predictive power of stream gains (Table 1). This highlights potential differences between plot, hillslope, and watershed scale studies. Findings of one may not easily translate to the other, calling to our attention the importance of understanding the scaling of streamflow generation mechanisms.

5.1.2. The Role of Stream Geomorphology for Gross Losses From the Channel to the Valley

Because the streams of the TCEF are high gradient, low-sinuosity, and the beds have coarse substrate with stable channel geometry (very little bed-load transport) the primary type of exchange in this system was that driven by differences in total hydraulic head; as indicated by the significant negative relationship between the normalized count of steps in each reach and volumetric loss (Figure 8). The interaction between streams and the hyporheic zone were likely driven by total head gradients that are dictated by differences in elevation of the water surface due to longitudinal streambed topography [*Harvey and Bencala*, 1993]. While other types of hyporheic exchange [*Wondzell and Gooseff*, 2013] could have played a role in how much water was lost to valley flow paths, the number of steps creating a higher hydraulic head appears to be the primary driver of stream losses in the reaches investigated at the TCEF. This suggested that once water entered the stream and valley system from the uplands (Figure 7), it was the topography of the streambed itself that promoted local losses from the stream to the valley and ultimately contributed to changes in net Q at the bottom of the reach (Figure 6).

Losses due to changes in head over steps can be considered vertical losses from the stream into the bed, and appear to be the main mechanism of exchange in high gradient, rocky stream types such as the TCEF [*Wondzell*, 2006]. Transient exchange could also play a role at different points in the season depending on the height of the stream surface relative to the height of the adjacent riparian water table [*Harvey and Bencala*, 1993; *Lewandowski et al*., 2009]. During snowmelt when channel water surface elevation and riparian water tables are high, horizontal losses could occur due to overbank flow and activation of side channels [*Poole et al*., 2006]. These processes might explain some of the increased variability that we observe about the relationship between steps and gross loss during our highest flow measurements (Figure 8a). Interestingly, the measurement period where steps had the least explanatory power was not the highest or lowest flow, but during the late snowmelt recession at 70 L/s (Figure 8c). We hypothesize that at this point, hydrologic connectivity between hillslopes and valley bottoms decreased, resulting in riparian water level declines and decreased near stream hydraulic gradients. This could contribute to increased horizontal exchange as valley flow paths evolve in a downstream direction and water tables and stream stage approach equilibrium [*Harvey et al*., 1996]. Once conditions approached steady state during base flow, there was a significant relationship between the normalized count of steps and volumetric loss of stream water (Figure 8d).

Across all scales, from a reach to an entire stream network, geologic structure and valley bottom morphology can be significant controls on the gross channel water balance [*Wondzell*, 2006; *Covino et al*., 2011; *Mallard et al*., 2014]. Our results suggested a strong linkage between the propensity for volumetric loss and the spatial patterns of stream morphology. In the upper portions of the watershed underlain by sandstone, there were fewer steps per 100 m of stream and less change in elevation ($<$5 m lost over the entire reach). This resulted in less volumetric loss from these upper reaches relative to lower reaches, particularly at the highest and lowest measured flow states (Figures 8a and 8d). Conversely, lower in the watershed where reaches are underlain by gneiss, the valley and channel slopes were much steeper. There were more steps and more elevation loss creating higher hydraulic heads and increased gross loss from these reaches (Figure 8). The structure of the channel evolved moving from the headwaters with sandstone lithology to the outlet with gneiss and gross loss evolved with it in a predictable way across all flow states. This suggests a strong linkage between valley bottom topographic structure influenced by underlying geology, stream morphology, and hydrologic exchange dynamics.

5.2. Implications

One major focus of hydrologic research has been how the organization of landscape structure leads to variability in the sources and timing of streamflow within and across watersheds. Every watershed, hillslope, and valley system is unique, which is true even for adjacent watersheds in the same geomorphic setting at the TCEF. However, this work provides insight into the dominant influences on exchange between hillslopes, underlying lithology, valley systems, and streams across spatial scales and flow states. We provide evidence for how geology and vegetation can influence the yield from one contributing area to the next (Figure 7), a critical consideration for model selection and parameter identification [*Wagener and Wheater*, 2006]. The addition of bedrock, topography, vegetation, and valley bottom controls on event and base flow contributions to streams may improve

our ability to constrain spatially explicit predictions of streamflow generation in ungauged basins [*Sivapalan*, 2003]. Additionally, our multiscale analyses highlight the spatial scales at which local and nonlocal watershed characteristics may control water delivery to streams [*Blöschl and Sivapalan*, 1995].

This research provides a link between network scale hydrologic exchange and the uplands of the watershed. In hillslope or small watershed hydrologic studies, bedrock is often considered a no-flow boundary [*Kampf and Burges*, 2007]. However, we know that shallow subsurface flow can recharge deeper geologic flow paths [*Generaux et al*., 1993], as indicated by bedrock type dependent yields to steams and the contributions of seeps and springs [*Tague and Grant*, 2004; *Jencso and McGlynn*, 2011; *Creutzfeldt et al*., 2014]. Under changing climate, it will be increasingly important to identify the spatial distribution of geologic sources and sinks of streamflow, storage capacity, and interactions with the shallow subsurface and valley bottoms in order to estimate watershed sensitivity to future conditions [*Tague and Grant*, 2004].

Improved understanding of gross gains and hydrologic exchange along a stream network can also help improve our understanding and interpretation of watershed biogeochemistry. Often, field studies of hydrologic exchange only consider one or two reaches and rarely incorporate continuous reaches across a stream network [e.g., *Triska et al*., 1989; *Harvey and Bencala*, 1993; *Ward et al*., 2014]. Previous spatially distributed network scale estimates of exchange and nutrient uptake have been developed using modeled or extrapolated discharge and velocity [e.g., *Mallard et al*., 2014; *Hall et al*., 2013]. Our direct measurements of hydrologic exchange made across an entire watershed and through a range of flow states (Figure 6) allowed us to relate these dynamics more directly to the physical structure of a watershed: both the uplands (Figure 7) and the valley system (Figure 8). Joint consideration of upland and valley bottom influences on exchange may help to improve stream network scale estimates of nutrient cycling through explicit accounting of hydrologic turnover using easily measured parameters. This can be used to advance our understanding of valley function [*Hayashi and Rosenberry*, 2002] and the role of hillslopes and riparian zones for buffering volumetric contributions and chemical signatures along the stream network [*McGlynn et al*., 2004; *Jencso et al*., 2010].

6. Conclusion

We measured streamflow at high spatial and temporal resolution in five watersheds in the TCEF in order to understand how streamflow scales with watershed area across flow states as well as the dominant watershed characteristics influencing these relationships. We found that discharge scaled with contributing area only at the larger watershed scales and that the quality of the relationship degraded with decreasing flow state. Reach net discharge could not be accounted for based on lateral contributing area alone because the net discharge does not account for the total amount of water entering and leaving the reach. However, using the gross channel water balance, we were better able to constrain topographic, geologic and vegetation influences on streamflow dynamics. The reach lateral contributing area and its vegetation and underlying lithology strongly correlated to gross gains to the channel network. Lateral contributing area and underlying geology related to the magnitude and duration of hydrologic connectivity between uplands and the stream. More densely vegetated areas had slightly higher gross gains during late base flow. Gross losses were influenced by the local channel topography and head drops that promote loss of surface water to valley flow paths. These findings help connect reach scale processes within channel networks to larger scale watershed storage and streamflow dynamics. Additionally, we have provided evidence of how large scale watershed characteristics such as topography and geology can influence small-scale stream exchange with the valley bottom. This contributed to our understanding of processes influencing the variability of stream flow dynamics, both delivery of water to the streams from the uplands as well as in-channel hydrologic exchange, across spatial scales and flow states.

Acknowledgments
Financial support for this project was provided by grants from the U.S. Department of Agriculture McIntire Stennis Program awarded to Jencso and a National Science Foundation Graduate Research Fellowship Program award to Bergstrom. Additionally, it builds on infrastructure and research from National Science Foundation Program awards EAR-0337650, EAR-0943640, and EAR-0837937 to McGlynn. We would like to thank Kaitlin Hayes and Tyler Smith for assistance with fieldwork. The authors appreciate significant field and logistical support from the USDA Forest Service Rocky Mountain Research Station. The data and analysis in this article can be acquired by contacting K. Jencso.

References

Anderson, M., and T. Burt (1978), Role of topography in controlling throughflow generation, *Earth Surf. Processes Landforms*, *3*(4), 331–344.
Bencala, K. E., M. N. Gooseff, and B. A. Kimball (2011), Rethinking hyporheic flow and transient storage to advance understanding of stream-catchment connections, *Water Resour. Res.*, *47*, W00H03, doi:10.1029/2010WR010066.
Beven, K., and M. Kirkby (1979), A physically based, variable contributing area model of basin hydrology, *Hydrol. Sci. Bull.*, *24*(1), 43–69.
Blöschl, G., and M. Sivapalan (1995), Scale issues in hydrological modelling: A review, *Hydrol. Processes*, *9*, 251–290.
Bonell, M. (1998), Selected challenges in runoff generation research in forests from the hillslope to headwater drainage basin scale, *J. Am. Water Resour. Assoc.*, *34*, 765–786.

Covino, T. P., and B. L. McGlynn (2007), Stream gains and losses across a mountain-to-valley transition: Impacts on watershed hydrology and stream water chemistry, *Water Resour. Res.*, *43*, W10431, doi:10.1029/2006WR005544.
Covino, T., B. McGlynn, and J. Mallard (2011), Stream-groundwater exchange and hydrologic turnover at the network scale, *Water Resour. Res.*, *47*, W12521, doi:10.1029/2011WR010942.
Creutzfeldt, B., P. Troch, A. Gunter, T. P. A. Ferre, T. Graeff, and B. Merz (2014), Storage-discharge relationships at different catchment scales based on local high-precision gravimetry, *Hydrol. Processes*, *28*, 1465–1475.
Day, T. J. (1976), Precision of salt dilution gauging, *J. Hydrol.*, *31*(34), 293–306.
D'Odorico, P., and R. Rigon (2003), Hillslope and channel contributions to the hydrologic response, *Water Resour. Res.*, *39*(5), 1113, doi:10.1029/2002WR001708.
Dooge, J. C. I. (1986), Looking for hydrologic laws, *Water Resour. Res.*, *22*(9S), 46S–58S.
Eaton, B., M. Church, and D. Ham (2002), Scaling and regionalization of flood flows in British Columbia, Canada, *Hydrol. Processes*, *16*, 6245–3263.
Emanuel, R. E., H. E. Epstein, B. L. McGlynn, D. L. Welsch, D. J. Muth, and P. D'Odorico (2010), Spatial and temporal controls on watershed ecohydrology in the northern Rocky Mountains, *Water Resour. Res.*, *46*, W11553, doi:10.1029/2009WR008890.
Emanuel, R. E., A. Hazen, B. L. McGlynn, and K. G. Jencso (2013), Vegetation and topographic influences on the connectivity of shallow groundwater between hillslopes and streams. *Ecohydrology*, *7*, 887–895.
Exner-Kittridge, M., J. L. Salinas, and M. Zessner (2014), An evaluation of analytical stream to groundwater exchange models: A comparison of gross exchanges based on different spatial flow distribution assumptions, *Hydrol. Earth Syst. Sci.*, *18*, 2715–2734.
Farnes, P. E., and W. W. McCaughey (1995), Hydrologic and geologic characterization of Tenderfoot Creek Experimental Forest, Montana, *Final Rep. RJVA-INT-92734*, 200 p., For. Sci. Lab., Mont. State Univ., Bozeman.
Freer, J., J. J. McDonnell, K. J. Beven, N. E. Peters, D. A. Burns, R. P. Hooper, B. Aulenbach, and C. Kendall (2002), The role of bedrock topography on subsurface storm flow, *Water Resour. Res.*, *38*(12), 1269, doi:10.1029/2001WR000872.
Gabrielli, C., J. J. McDonnell, and T. Jarvis (2012), The role of bedrock groundwater in rainfall-runoff response at hillslope and catchment scales, *J. Hydrol.*, *450–451*, 117–133.
Gannon, J. P., S. W. Bailey, and K. J. McGuire (2014), Organizing groundwater regimes and response thresholds by soils: A framework for understanding runoff generation in a headwater catchment, *Water Resour. Res.*, *50*, 8403–8419, doi:10.1002/2014WR015498.
Generaux, D. P., H. F. Menond, and P. J. Mulholland (1993), Spatial and temporal variability in streamflow generation on the West Fork of Walker Branch watershed, *J. Hydrol.*, *142*, 137–166.
Graham, C., H. Barnard, W. van Verseveld, and J. J. McDonnell (2010), Estimating the deep seepage component of the hillslope and catchment water balance within a measurement uncertainty framework. *Hydrol. Processes*, *24*, 3631–3647.
Gupta, V. K., O. J. Mesa, and D. R. Dawdy (1994), Multiscaling theory of flood peaks: Regional quantile analysis, *Water Resour. Res.*, *30*(12), 3405–3421.
Gupta, V. K., S. L. Castro, and T. M. Over (1996), On scaling exponents of spatial peak flows from rainfall and river network geometry, *J. Hydrol.*, *187*, 81–104.
Hall, R. O., M. A. Baker, E. J. Rosi-Marshall, J. L. Tank, and J. D. Newbold (2013), Solute-specific scaling of inorganic nitrogen and phosphorous uptake in streams, *Biogeosciences*, *10*, 7323–7331.
Harvey, J., B. Wagner, and K. Bencala (1996), Evaluating the reliability of the stream tracer approach to characterize stream-subsurface water exchange, *Water Resour. Res.*, *32*(8), 2441–2451.
Harvey, J. W., and K. E. Bencala (1993), The effect of streambed topography on surface-subsurface water exchange in mountain catchments, *Water Resour. Res.*, *29*(1), 89–98.
Hayashi, M., and D. O. Rosenberry (2002), Effects of groundwater exchange on the hydrology and ecology of surface water, *Groundwater*, *40*(3), 309–316.
Hewlett, J. D., and A. R. Hibbert (1967), Factors affecting the response of small watersheds to precipitation in humid areas, in *Forest Hydrology*, edited by W. E. Sopper and H. W. Lull, pp. 275–291, Pergamon Press, N. Y.
Holdorf, H. D. (1981), Soil resource inventory: Lewis and Clark National Forest interim in-service report, Lewis and Clark Natl. For., For. Supervisor's Off., Great Falls, Mont.
Hood, S. M., H. Y. Smith, D. K. Wright, and L. S. Glasgow (2012), Management guide to ecosystem restoration treatments: Two-aged lodgepole pine forests of Central Montana, USA, *Gen. Tech. Rep. RMRS-GTR-294*, Rocky Mt. Res. Stn., U. S. For. Serv., Fort Collins, Colo.
Hornberger, G. M., J. P. Raffensperger, P. L. Wiberg, and K. N., Eshleman (1998), *Elements of Physical Hydrology*, Johns Hopkins University Press, Baltimore, Md.
Horton, R. E. (1914), Discussion on yield of drainage-areas, *J. N. Engl. Water Works Assoc.*, *28*(4), 538–539.
Huff, D. D., R. V. O'Neill, W. R. Emanuel, J. W. Elwood, and J. D. Newbold (1982), Flow variability and hillslope hydrology, *Earth Surf. Processes Landforms*, *7*, 91–94.
Jencso, K., B. McGlynn, M. Gooseff, S. Wondzell, K. Bencala, and L. Marshall (2009), Hydrologic connectivity between landscapes and streams: Transferring reach-and plot-scale understanding to the catchment scale, *Water Resour. Res.*, *45*, W04428, doi:10.1029/2008WR007225.
Jencso, K. G., B. L. McGlynn, M. N. Gooseff, K. E. Bencala, and S. M. Wondzell (2010), Hillslope hydrologic connectivity controls riparian groundwater turnover: Implications of catchment structure for riparian buffering and stream water sources, *Water Resour. Res.*, *46*, W10524, doi:10.1029/2009WR008818.
Jencso, K. G., and B. L. McGlynn (2011), Hierarchical controls on runoff generation: Topographically driven hydrologic connectivity, geology, and vegetation, *Water Resour. Res.*, *47*, W11527, doi:10.1029/2011WR010666.
Kampf, S. K., and S. J. Burges (2007), A framework for classifying and comparing distributed hillslope and catchment hydrologic models, *Water Resour. Res.*, *43*, W05423, doi:10.1029/2006WR005370.
Kennedy, V. C., A. P. Jackman, S. M. Zand, G. W. Zellweger, and R. J. Avanzino (1984), Transport and concentration controls for chloride, strontium, potassium, and lead in Uvas Creek, a small cobble bed stream in Santa Clara County, California, U.S.A. 1. Conceptual model, *J. Hydrol.*, *75*, 67–110.
Kilpatrick, F. A., and E. D. Cobb (1985), Measurement of discharge using tracers, *U.S. Geol. Surv. Tech. Water Resour. Invest.*, *Book 3*, *Chap. A16.*
Lewandowski, J., Lischeid, G., and Nützmann, G. (2009), Drivers of water level fluctuations and hydrological exchange between groundwater and surface water at the lowland River Spree (Germany): Field study and statistical analyses. *Hydrol. Processes*, *23*, 2117–2128.
Mallard, J. M., B. McGlynn, and T. P. Covino (2014), Lateral inflows, stream-groundwater exchange, and network geometry influence stream-water composition, *Water Resour. Res.*, *50*, 4603–4623, doi:10.1002/2013WR014944.
McDonnell, J. J., M. Sivapalan, K. Vache, S. Dunn, G. Grant, R. Haggerty, C. Hinz, R. Hooper, J. Kirchner, M. L. Roderick, J. Selker, and M. Weiler (2007), Moving beyond heterogeneity and process complexity: A new vision for watershed hydrology, *Water Resour. Res.*, *43*, W07301, doi:10.1029/2006WR005467.

McGlynn, B. L., and J. Seibert (2003), Distributed assessment of contributing area and riparian buffering along stream networks, *Water Resour. Res.*, *39*(4), 1082, doi:10.1029/2002WR001521.
McGlynn, B. L., J. J. McDonnell, J. Seibert, and C. Kendall (2004), Scale effects on headwater catchment runoff timing, flow sources, and groundwater-streamflow relations, *Water Resour. Res.*, *40*, W07504, doi:10.1029/2003WR002494.
Mincemoyer, S. A., and J. L. Birdsall (2006), Vascular flora of the Tenderfoot Creek Experimental Forest, Montana, *Madrono*, *53*(3), 211–222.
Montgomery, D. R., and J. M. Buffington (1997), Channel-reach morphology in mountain drainage basins, *GSA Bull.*, *109*(5), 596–611.
Nippgen, F., B. L. McGlynn, L. A. Marshall, and R. E. Emanuel (2011), Landscape structure and climate influences on hydrologic response, *Water Resour. Res.*, *47*, W12528, doi:10.1029/2011WR011161.
Nippgen, F., B. L. McGlynn, and R. E. Emanuel (2015), The spatial and temporal evolution of contributing areas, *Water Resour. Res.*, *51*, 4550–4573, doi:10.1002/2014WR016719.
O'Callaghan, J., and D. Mark (1984), The extraction of drainage networks from digital elevation data, *Comput. Vision Graph. Image Process.*, *28*(3), 323–344.
Onda, Y., Y. Komatsu, M. Tsujimura, and J.-I. Fujihara (2001), The role of subsurface runoff through bedrock on storm flow generation, *Hydrol. Processes*, *15*, 1693–1706.
Payn, R., M. Gooseff, B. McGlynn, K. Bencala, and S. Wondzell (2009), Channel water balance and exchange with subsurface flow along a mountain headwater stream in Montana, United States, *Water Resour. Res.*, *45*, W11427, doi:10.1029/2008WR007644.
Payn, R. A., M. N. Gooseff, B. L. McGlynn, K. E. Bencala, and S. M. Wondzell (2012), Exploring changes in the spatial distribution of stream baseflow generation during a seasonal recession, *Water Resour. Res.*, *48*, W04519, doi:10.1029/2011WR011552.
Poole, G. C., J. A. Stanford, S. W. Running, and C. A. Frissell (2006), Multiscale geomorphic drivers of groundwater flow paths: Subsurface hydrologic dynamics and hyporheic habitat diversity, *J. North Am. Benthological. Soc.*, *25*(2), 288–303.
Porporato, A., E. Daly, and I. Rodriguez-Iturbe (2004), Soil water balance and ecosystem response to climate change, *Am. Nat.*, *164*(5), 625–632.
Reynolds, M. (1995), Geology of Tenderfoot Creek Experimental Forest, Little Belt Mountains, Meagher County, Montana, in *Hydrologic and Geologic Characteristics of Tenderfoot Creek Experimental Forest, Montana*, *Final Rep. RJVA-INT-782 92734*, edited by P. Farnes, Intermt. Res. Stn., For. Serv., U.S. Dept. of Agric., Bozeman, Mont.
Rodriguez-Iturbe, I., and A. Porporato (2004), *Ecohydrology of water-controlled ecosystems, in Soil Moisture and Plant Dynamics*, Cambridge Univ. Press, Cambridge, U. K.
Sauer, V. B., and D. P. Turnipseed (2010), Stage measurement at gaging stations, *U.S. Geol. Surv. Tech. Methods*, *Book 3*, *Chap. A7*, 45 pp.
Schmidt, W. C., and J. L. Friede (1996), Experimental forests, ranges, and watersheds in the northern Rocky mountains: A compendium of outdoor laboratories in Utah, Idaho, and Montana, *Gen. Tech. Rep. INT-GTR-334*, Interm. Res. Stn., U.S. For. Serv., Ogden, Utah.
Seyfried, M. S., and B. P. Wilcox (1995), Scale and the nature of spatial variability: Field examples having implications for hydrologic modeling, *Water Resour. Res.*, *31*(1), 173–184.
Sidle, R. C., Y. Tsuboyama, S. Noguchi, I. Hosoda, M. Fujieda, and T. Shimizu (2000), Stormflow generation in steep forested headwaters: A linked hydrogeomorphic paradigm, *Hydrol. Processes*, *14*(3), 369–385.
Sivapalan, M. (2003), Prediction in ungauged basins: A grand challenge for theoretical hydrology. *Hydrol. Processes*, *17*, 3163–3170.
Smith, J. A. (1992), Representation of basin scale in flood peak distributions, *Water Resour. Res.*, *28*(11), 2993–2999.
Smith, T., L. Marshall, B.L. McGlynn, and K. Jencso (2013), Using field data to inform and evaluate a new model of catchment hydrologic connectivity, *Water Resour. Res.*, *49*, 6834–6846, doi:10.1002/wrcr.20546.
Soulsby, C., P. Rodgers, J. Petry, D. M. Hannah, I. A. Malcolm, and S. M. Dunn (2004), Using tracers to upscale flow path understanding in mesoscale mountainous catchments: Two examples from Scotland, *J. Hydrol.*, *291*, 174–196.
Soulsby, C., D. Tetzlaff, P. Rodgers, S. Dunn, and S. Waldron (2006), Runoff processes, stream water residence times, and controlling landscape characteristics in a mesoscale catchment: An initial evaluation, *J. Hydrol.*, *325*(1–4), 197–221.
Tague, C., and G. E. Grant (2004), A geological framework for interpreting the low-flow regimes of Cascade Streams, Willamette River Basin, Oregon, *Water Resour. Res.*, *40*, W04303, doi:10.1029/2003WR002629.
Tetzlaff D., C. Birkel, J. Dick, J. Geris, and C. Soulsby (2014), Storage dynamics in hydropedological unit control hillslope connectivity, runoff generation, and the evolution of catchment transit time distributions, *Water Resour. Res.*, *50*, 969–985, doi:10.1002/2013WR014147.
Toth, J. A. (1963), A theoretical analysis of groundwater flow in small drainage basins, *J. Geophys. Res.*, *68*(16), 4375–4387.
Triska, F. J., V. C. Kennedy, R. J., Avanzino, G. W. Zellweger, and K. E. Bencala (1989) Retention and transport of nutrients in a third-order stream in northwestern California: Hyporheic processes, *Ecology*, *70*(6), 1893–1905.
Tromp-van Meerveld, H. J., and J. J. McDonnell (2006), Threshold relations in subsurface stormflow: 1. A 147-storm analysis of the Panola hillslope, *Water Resour. Res.*, *42*, W02410, doi:10.1029/2004WR003778.
Tromp-van Meerveld, H. J., N. E. Peters, and J. J. McDonnell (2007), Effect of bedrock permeability on subsurface stormflow and the water balance of a trenched hillslope at the Panola Mountain Research Watershed, Georgia, USA, *Hydrol. Processes*, *21*(6), 750–769.
Uchida, T., Y. Asano, Y. Onda, and S. Miyata (2005), Are headwaters just the sum of hillslopes?, *Hydrol. Processes*, *19*, 3251–3261.
Vidon, P., and A. P. Smith (2007), Upland controls on the hydrological functioning of riparian zones in glacial till valleys of the Midwest, *J. Am. Water Resour. Assoc.*, *43*(6), 1524–1539.
Wagener, T., and H. S. Wheater (2006), Parameter estimation and regionalization for continuous rainfall-runoff models including uncertainty, *J. Hydrol.*, *320*, 132–154.
Wagner, T., M. Sivapalan, P. Troch, and R. Woods (2007), Catchment classification and hydrologic similarity, *Geogr. Compass 1*, 901–931.
Ward, A. S., M. Fitzgerald, M. N. Gooseff, T. J. Voltz, A. M. Binley, and K. Singha (2012), Hydrologic and geomorphic controls on hyporheic exchange during base flow recession in a headwater mountain stream, *Water Resour. Res.*, *48*, W04513, doi:10.1029/2011WR011461.
Ward, A. S., M. N. Gooseff, M. Fitzgerald, T. J. Voltz, and K. Singha (2014), Spatially distributed characterization of hyporheic solute transport during baseflow recession in a headwater mountain stream using electrical geophysical imaging, *J. Hydrol.*, *517*, 362–377.
Wondzell, S. M. (2006), Effect of morphology and discharge on hyporheic exchange flows in two small streams in the Cascade Mountains of Oregon, USA, *Hydrol. Processes*, *20*, 267–287.
Wondzell, S. M., and M. N. Gooseff (2013), Geomorphic controls on hyporheic exchange across scales: Watersheds to particles, in *Treatise on Geomorphology*, vol. 9, edited by J. Shroder and E. Whol, pp. 203–218, Academic, San Diego, Calif.
Wood, E. F., M. Sivapalan, K. Beven, and L. Band (1988), Effects of spatial variability and scale with implications to hydrologic modeling, *J. Hydrol.*, *102*(1–4), 29–47.
Yue, S., and T. Y. Gan (2009), Scaling properties of Canadian flood flows, *Hydrol. Processes*, *23*, 245–258.
Zellweger, G. W., R. J. Avanzino, and K. E. Bencala (1989), Comparison of tracer-dilution and current-meter discharge measurements in a small gravel-bed stream, Little Lost Man Creek, California, *U.S. Geol. Surv. Water Resour. Invest. Rep.*, 89-4150.